Characterization of NbC and (Nb,Ti)N nanoprecipitates in TRIP assisted multi phase steels

G. K. Tirumalasetty[1,2,*], M.A. van Huis[1,3], C.M. Fang[1,2], Q. Xu[1,3], F.D. Tichelaar[1],

D.N. Hanlon[4], J. Sietsma[5], H.W. Zandbergen[1].

[1]*Kavli Institute of Nanoscience, Delft University of Technology,*

Lorentzweg 1, 2628 CJ Delft, The Netherlands

[2]*Materials innovation institute (M2i), Mekelweg 2, 2628 CD Delft, The Netherlands*

[3]*EMAT, University of Antwerp, Groenenborgerlaan 171, 2020 Antwerp, Belgium.*

[4] *Tata Steel Research Development and Technology, P.O. Box 10.000,*

1970 CA IJmuiden, The Netherlands

[5] *Department of Materials Science and Engineering, Delft University of Technology,*

Mekelweg 2, 2628 CD Delft, The Netherlands

[*]Corresponding author:

Address: Kavli Institute of Nanoscience,

Delft University of Technology,

Lorentzweg 1, 2628 CJ Delft,

The Netherlands

Email: g.k.tirumalasetty@tudelft.nl.

Tel./ fax: +31 15 2781536 / +31 15 2786600

Abstract

Multiphase steels utilising composite strengthening may be further strengthened via grain refinement or precipitation by the addition of microalloying elements. In this study a Nb microalloyed steel comprising martensite, bainite and retained austenite has been studied. By means of transmission electron microscopy (TEM), we have investigated the size distribution and the structural properties of (Nb,Ti)N and NbC precipitates, their occurrence in the various steel phases, and their relationship with the Fe matrix. (Nb,Ti)N precipitates were found in ferrite, martensite, and bainite, while NbC precipitates were found only in ferrite. All NbC precipitates were found to be small (5 – 20 nm in size) and to have a face centred cubic crystal structure with lattice parameter $a = 4.36 \pm 0.05$ Å. In contrast, the (Nb,Ti)N precipitates were found in a broader size range (5 – 150 nm) and to have a face centred cubic crystal structure with lattice parameter $a = 8.09 \pm 0.05$ Å. While the NbC precipitates were found to be randomly oriented, the (Nb,Ti)N precipitates have a well-defined Nishiyama Wasserman (N-W) orientation relationship with the ferrite matrix. An analysis of the lattice mismatch suggests that the latter precipitates have a high potential for effective strengthening. DFT calculations were performed for various stoichiometries of NbC_X and $Nb_XTi_YN_Z$ phases and the comparison with experimental data indicates that both the carbides and nitrides are deficient in C and N content.

Keywords: Multi phase steel, NbC, (Nb,Ti)N, precipitation, transmission electron microscopy

1. Introduction

High-strength steels can achieve a good balance of strength and ductility by utilising combinations of grain refinement, precipitation strengthening, and composite strengthening. Modern multi phase (MP) steels rely primarily on grain refinement and composite hardening. However, microalloying additions may provide effective means for further strengthening via enhanced grain refinement and/or precipitation. The role of microalloying additions in multiphase steels requires further clarification. Many investigations have focused on the role of Nb [1-4] in steels. NbC precipitates are formed during the hot-rolling process, which reduces the size of the recrystallized grains by pinning the grain boundaries and refines the final microstructure resulting in the increase in yield strength and tensile strength. These precipitates also form an obstacle for the movement of dislocations [5] and increase in strength is achieved while maintaining good toughness.

In steels containing both Nb and Ti, it was observed that there was a delay in precipitation of NbC due to formation of stable (Nb,Ti)(C,N) [6]. Wang et al. [7] observed that a thermo-mechanical heat treatment transformed the (Nb,Ti)(C,N) precipitates from cubical shape to rectangular shapes. In other investigations, it was found [8,9] that deformation during a hot-rolling process accelerates the precipitation of NbC and (Nb,Ti)(C,N) precipitates. Weiss et al. [10] observed that 5% pre-strain increased the rate of precipitation of NbC precipitates by about one order of magnitude. Recently Moon et al. [9] investigated the effect of stress state (tensile, compressive stress) on the coarsening behaviour of (Nb,Ti)(C,N) particles during a thermo-mechanical treatment. Their results showed that the compressive stress was more effective than tensile stress.

The main aim of the current work is to structurally characterize the nanosized precipitates of NbC and (Nb,Ti)N in a multi-phase (MP) steel containing fractions of bainite (B), martensite (M) and retained austenite (RA) in a predominantly ferritic matrix. Particular attention has been paid to assessing the precipitation state in the individual phases.

2. Experimental Procedure

The chemical composition of the Nb-alloyed MP steel used in the present work is listed in Table 1. The material is produced on an industrial hot dip galvanising line using a conventional intercritical annealing cycle as is standard practice for dual phase (DP) and transformation induced plasticity (TRIP) steels. The microstructures were studied by optical microscopy (OM) and transmission electron microscopy (TEM). A stepped etching procedure was followed to reveal the optical microstructure [11]. Electron transparent TEM samples were made using standard electropolishing to reveal various phases in the TEM microstructures. The specimens for electropolishing were pre-thinned by grinding along the transverse direction using SiC paper with roughness from 350 down to 4000. Electropolishing was carried out in a twin-jet polisher using 5 percent perchloric acid solution at a temperature of -20^0C. TEM analysis was performed using a Philips CM30T and a FEI Tecnai F20ST/STEM microscope operating at 300 and 200 kV, respectively, to identify microstructure and precipitates. Selected Area Diffraction (SAD) was used to distinguish different phases and to characterize the precipitates in this steel and the orientations of the diffraction patterns were defined with respect to the electron beam. The analytical methods of

energy dispersive X-ray spectroscopy (EDX) and electron energy loss spectroscopy (EELS) were employed to investigate chemical compositions.

3. Results and Discussion

The microstructure of the steel studied in this work contains multiple phases (ferrite, martensite, retained austenite and bainite). The precipitation behaviour of (Nb,Ti)(C,N) carbonitrides can be expected to be different in the different phases within the steel, primarily because of different solubilities and mobilities of the alloying elements in these phases. Therefore, we first discuss briefly the general microstructure before showing the TEM results on the occurrence and type of precipitates found in the various phases.

3.1 Light microscopic analysis of microstructures

The typical microstructure of the steel is shown in Figure 1, in which the large brown areas represent ferrite, and the fine dark and grey areas represent bainite. Martensite is generally etched in a straw tint colour and retained austenite is of white colour in the optical micrograph [11]. The fractions of retained austenite, ferrite martensite and bainite in Figure 1 were quantified using Image analyser. The retained austenite constitutes 2.88% while martensite bainite and ferrite constitute 3.9%, 6.49% and 77.07% of the area fractions respectively. It can be seen from Figure 1 that the average ferrite grain size of Nb-containing MP steels is about $5\,\mu m$, which is small in comparison with intercritically annealed Dual Phase steel [12]. Furthermore, the fractions of bainite and martensite are considerably higher while the fractions of retained austenite are lower than TRIP-aided Dual Phase steel [12].

5

3.2 TEM analysis of microstructures

In order to investigate the precipitation in conjunction with the presence of the various phases, grains of each of the phases were inspected for the presence of precipitates using TEM. The analysis was carried out on more than 15 bulk samples that were thinned for electron transparency. In combination, the total volume probed by means of TEM is about 7500 μm^3. The results displayed below are typical examples of observations that were found throughout the analyses. Table 2 gives an overview of the occurrence of the precipitates in the steel phases.

Figure 2 shows a grain of ferrite. The TEM micrograph shows a pole where diffraction bands meet corresponding to the $(1\bar{1}1)$ orientation of ferrite as identified by electron diffraction (inset in Figure 2). The ferrite grain is bent because of the thinning required for TEM analysis. The ferrite grain contains precipitates with different size ranges: coarse precipitates in size range of 100-150 nm, medium-sized precipitates in size range of 50-60 nm and fine precipitates with a size of 10–20 nm as shown in the schematic representation in Figure. 2.

Considering the austenite phase, two types of grains were found in this steel: blocky type retained austenite grains, and filmy type austenite plates. The blocky type retained austenite grains in Figure. 3 had an angular deviation of 5.3 ± 0.2^{o} between $(001)_{\alpha}$ and $(1\bar{1}0)_{\gamma}$ planes and was found near to the Nishiyama Wasserman (N-W) relationship commonly seen between the fcc (face centred cubic, γ-Fe) and bcc (body centred cubic, α-Fe) phases in metallic materials [13]. The N-W relationship is defined by

6

$$(110)_{\alpha} \parallel (111)_{\gamma} \text{ and } [001]_{\alpha} \parallel [1\bar{1}0]_{\gamma} \tag{1}$$

Figure 4 shows a filmy type austenite grain with a neighbouring ferrite grain and Figure 5a shows a grain of bainite and filmy austenite surrounded by a ferrite grain. The angular deviation between the neighbouring ferrite grain and filmy type austenite was $0.5 \pm 0.2^{\circ}$ between $(111)_{\alpha}$ and $(110)_{\gamma}$, which is close to the Kurdjumov Sachs (K-S) relationship [13]. The K-S relationship is defined by

$$(0\bar{1}1)_{\alpha} \parallel (111)_{\gamma} \text{ and } [111]_{\alpha} \parallel [1\bar{1}0]_{\gamma} \tag{2}$$

Alternate regions of ferrite and austenite were seen with a plate thickness of the order of a few hundred nanometers and surrounded by dislocation loops. No precipitates were found in either the blocky type austenite grains or in filmy type austenite grains. (Nb,Ti)N precipitates were found, though, in the bainitic ferrite plates. These precipitates were faceted in shape and were found inside the bainitic ferrite and in adjacent ferrite grains as in Figure. 5a.

The fourth phase (besides ferrite, austenite and bainite) is martensite. Figure 5b shows a martensite grain (α') where the lathes are oriented along the $(3\bar{3}1)$ orientation. (Nb,Ti)N precipitates can be observed in these martensite grains, and reflections are found in the diffraction pattern, which originate from the precipitates as shown in Figure. 5c.

3.3 Precipitates containing Nb and Ti

It is known that elements like Nb, V and Ti have a strong affinity for bonding with C and N. Consequently, microalloying additions of Nb, Ti and V to MP steel can lead to precipitation of Nb, Ti and V carbides and nitrides. TEM inspections of many areas show that this steel mainly contains (Nb,Ti)N precipitates with a size range of 10–150

7

nm. A dark-field recording using the $g=404$ reflection in the $[11\bar{1}]$ projection of (Nb,Ti)N is shown in Figure. 6a. Here (Nb,Ti)N precipitates can be observed which are in an $(11\bar{1})$ orientation inside the grain of ferrite that is in an $(1\bar{1}0)$ orientation, as is also clear from the corresponding diffraction pattern in Figure 6b. The precipitates are distributed throughout the material, and have a wide size dispersion. Figure 6c shows a large precipitate inside a ferrite grain. EDX analysis of the precipitate by converging the electron beam on the precipitate, shows a higher concentration of Ti in comparison with Nb. Different precipitates were found to have varying Ti/Nb atomic ratios (in a range of $2.4-4.5$). An average value for the Ti/Nb atomic ratio was determined from 7 larger precipitates as 2.83 ± 0.81. In the EDX analysis, minor contributions from Al, Si, S, Mn, Fe and Cr also appear in these precipitates since the EDX signal in TEM comes not only from the precipitate but also from the matrix phase surrounding the precipitate, as a large part of the sample is hit by stray electrons. EELS analysis (Electron Energy Loss Spectroscopy) was also carried out on the same precipitates which showed the presence of N and but no evidence of C as shown in Figure. 7, indicating a $Nb_XTi_YN_Z$ type of precipitate. When combining the Ti/Nb ratio as obtained by means of EDX with the Ti/N ratio as found from EELS, the overall composition is approximately $Nb_{0.35}Ti_{1.0}N_{0.63}$.

In order to determine the unit cell, a large (Nb,Ti)N precipitate was chosen as shown in Figure 6c and a diffraction tilt series was performed in two orientations using selected area diffraction (SAD) as shown in Figure. 8a and Figure. 8b. The unit cell reconstructed from the tilt series is face centred cubic with lattice parameter $a = 8.09 \pm 0.05$ Å. In comparison, pure TiN and pure NbN are rocksalt phases (space group $Fm\bar{3}m$) with lattice parameters $a_{TiN}=4.27$ Å [32] and $a_{NbN}=4.44$ Å [33]. Therefore,

the experimentally found lattice parameter of 8.09 Å of the composite (Nb,Ti)N phase suggests a doubling of the rocksalt unit cell (i.e. a rocksalt superstructure with a certain (partial) ordering of the Nb and Ti atoms on the non-carbon sites). However, in that case the rocksalt lattice would be substantially compressed by 4-9% with respect to the pure NbN and TiN phases. Therefore, the possibility of a non-rocksalt type structure cannot be ruled out. In Section 3.5 below, results of density function theory (DFT) calculations will be presented for qualitative comparison with the experimental data in order to elucidate the crystal structure of the precipitates.

In Figure. 8b, the (Nb,Ti)N precipitate is in a $(\bar{1}1\bar{2})$ orientation. In the diffraction patterns in Figure 8a, the (Nb,Ti)N precipitate is in the $(\bar{1}11)$ orientation and the ferrite matrix is in the (011) orientation. Thus these (Nb,Ti)N precipitates have a *Nishiyama Wasserman (N-W)* orientation relationship with the ferrite matrix*:*

$$(011)\ \alpha\text{-Fe} \ // \ (\bar{1}11)\ (Nb,Ti)N \tag{3}$$

$$[100]\ \alpha\text{-Fe} \ // \ [110]\ (Nb,Ti)N \tag{4}$$

Other, smaller (Nb,Ti)N precipitates with very similar chemical composition were analysed as well and were found to have the same orientation relationship, so that this can be considered a general result for the (Nb,Ti)N/α-Fe precipitate-matrix system.

In Table 3, the experimentally determined lattice parameter of (Nb,Ti)N is listed, as well as the lattice mismatch calculated in three perpendicular directions. Here the lattice mismatch is calculated with Fe as a reference, $\eta = |(d_{(NbTi)N} - d_{Fe})/d_{Fe}|$. In one direction, [100]Fe//[110](NbTi)N, there is a good fit with a very small lattice mismatch ($0.0 \pm 1.1\%$). In the other two directions, the mismatch is large, 16% and

18%. The probability that a certain orientation relationship occurs, is determined by the interface energies that are associated with that orientation relationship. The interface energy can be considered to consist of two contributions: short-range contributions which are determined by the local, relaxed atomistic configuration at the interfaces, and long-range contributions such as strain in the embedding ferrite matrix caused by mismatch of the unit cells, which is sometimes partly relieved by misfit dislocations. The lattice mismatches as listed in Table 3 suggest that there is little strain in one direction, and considerable strain in the other two directions indicating that the orientation relationship is partially based on a semi-coherent interface. Such precipitates are more likely to effectively strengthen steels [14] than precipitates that have fully incoherent interfaces, which is expected for the NbC precipitates discussed below that have a random orientation relationship with the matrix.

3.4 Precipitates containing Nb and C

Also very small precipitates (5-20 nm) were observed in some grains of ferrite, as shown in Figure 9. The NbC precipitates were very close to each other and the EDX analysis confirmed higher concentrations of Nb and C than the surrounding ferrite matrix. From the literature [15-17], it is known that Nb can form $Nb(C,N)$, Fe_2Nb (Laves phase) and Fe_3Nb_3C (M_6C) particles in Nb-containing ferritic stainless steel. SAD was performed on these precipitates and it was found that these precipitates had a lattice parameter which was close to that of NbC (Figure 10). The NbC precipitates were identified as cubic with lattice parameter a=4.36 $\pm$ 0.05 Å. In contrast to the (Nb,Ti)N precipitates, the NbC precipitates were found in random orientations and thus have no preferred orientation relationship with the surrounding ferrite. In the literature [18], it is reported that the orientation relationship between NbC and ferrite

is cube-on-cube (which would result in a lattice mismatch of 23%, see Table 3), whereas no orientation relation was observed in the present work.

The fact that a minority (less than 10%) of the ferrite grains contained these NbC precipitates points to an inhomogeneous distribution of the alloying elements over the material, which leads to heterogeneous precipitation of these precipitates within a single phase. Also the heat treatment cycle might play a role in the precipitation behaviour. There are two types of ferrite which are formed during the heat treatment process; intercritical ferrite, which is formed at intercritical annealing temperatures, and bainitic ferrite, which is formed at bainitic temperatures. The precipitation in these two types of ferrite can be different. The observations that NbC precipitates are found only in ferrite grains as in Table 2 is in agreement with the observations by Pereloma *et al.* [2]. These NbC precipitates could have been formed in austenite [18] but were not observed in austenite grains at room temperature, suggesting that the ferrite grains might have nucleated at the carbon depleted NbC precipitate sites in austenite. These smaller precipitates which are uniformly distributed in the ferrite matrix with short inter-precipitate distances are known to cause dislocation pinning, leading to a substantial improvement in strength of this steel [5].

3.5 Density functional theory calculations

From the experiments, the lattice parameters and the space group of the (Nb,Ti)N phase were determined, however without a full determination of the crystal structure as the atomic positions were not resolved. Here we perform density functional theory (DFT) calculations in order to obtain more insight into the energetically most favourable stoichiometry and in order to investigate whether the composite phase

11

yields a smaller lattice parameter. Our experimental results on the (Nb,Ti)N precipitates show that the space group is $Fm\overline{3}m$, with a lattice parameter of 8.09 Å. This suggests a rocksalt superstructure with a lattice parameter that is approximately twice the lattice parameter of TiN, but smaller. The calculations were conducted employing the VASP code [20-22] within the projector-augmented wave (PAW) approach [23, 24] employing the generalized gradient approximation (GGA) with PBE potentials [25]. The cut-off energy of the wave functions was 500 eV, the cut-off energy of the augmentation functions was 645 eV. The electronic wave functions were sampled on a 12×12×12 grid in the irreducible Brillouin zone (BZ) of the $2a_0 \times 2a_0 \times 2a_0$ supercells (a_0 is the lattice parameter of a convention cell of NaCl-type structure), using the Monkhorst and Pack method [26]. The calculations were performed for a temperature of 0 K and for zero pressure. For the calculation of formation enthalpies, the solutes of Nb, Ti, N and C in bcc (ferrite) Fe were used as a reference. The enthalpies of the solutes were calculated using 54-atom bcc Fe supercells (dimensions $3a_{Fe} \times 3a_{Fe} \times 3a_{Fe}$), whereby Nb, Ti solutes are positioned at substitutional sites ($Fe_{53}Nb$, $Fe_{53}Ti$) while solutes of N and C are positioned at interstitial sites ($Fe_{54}N$, $Fe_{54}C$). The enthalpies of the solutes are then determined as $H^{sol}(M) = H(Fe_{53}M) - 53 \cdot H(Fe)$ for M=Nb,Ti and $H^{sol}(X) = H(Fe_{54}X) - 54 \cdot H(Fe)$ for X=C,N. It was verified that the cut-off energies and the density of the k-meshes were sufficiently high for good energy convergence (< 1 meV/atom). Although solution energies are not directly used in the current calculations, the enthalpy values of $H^{sol}(A)$ enable to calculate the corresponding solution energies for these elements in bcc Fe by subtracting the energy of the pure elements (bcc Nb, hcp Ti, the N_2 molecule, and graphite) as $\Delta E^{sol}(A) = H^{sol}(A) - H(A)$, where A=Nb,Ti,N,C. Solution energies for Nb, Ti, N and C in ferrite are then obtained as -0.135, -0.799, -0.006, and

0.582 eV, respectively. Here the reference energies $H(A)$ of graphite and N_2 were calculated as explained in Refs. [28-30].

For the precipitate phases, calculations were performed for different chemical compositions using different unit cells. For NbC_X, a conventional rocksalt (NaCl-type) cell was used with $0<x<1$, and for $Nb_X Ti_Y N_Z$ a supercell was used $(2a_0 \times 2a_0 \times 2a_0)$, whereby the Nb/Ti ratio was varied. Also the nitrogen content was varied within the composition $Nb_{0.25} Ti_{0.75} N_Z$ ($0<z<1$), as this composition is closest to the experimentally found Nb/Ti ratio. Structural optimisations were performed for both the lattice parameters and the relative atomic coordinates.

Two different definitions of formation energy were used to consider the relative stability of $Nb_X Ti_Y X_Z$ (X can be either N or C). The formation energy ΔH^1_{form} is defined with respect to the solutes of Nb, Ti, C, N in bcc Fe:

$$\Delta H^1_{form} = H(Nb_x Ti_y X_z) - [x \cdot H^{sol}(Nb) + y \cdot H^{sol}(Ti) + z \cdot H^{sol}(X)], \tag{5}$$

while the formation enthalpy ΔH^2_{form} is defined with respect to the pure compounds TiX, NbX (X=C,N) as

$$\Delta H^2_{form} = H(Nb_x Ti_y X_z) - z/(x+y) [x \cdot H(NbX) + y \cdot H(TiX)]$$
$$+ \{1 - z/(x+y)\} [x \cdot H^{sol}(Nb) + y \cdot H^{sol}(Ti)], \tag{6}$$

whereby the last term in Eq. (6) corrects for N or C deficiency (in case $z<x+y$).

Table 4 summarises the calculated lattice parameters and formation enthalpies of NbC, NbN, TiN and (Nb,Ti)N-type phases. The formation enthalpies are defined in Eqs. (5) and (6) above. Three groups of NbC and (Nb,Ti)N precipitates are considered whereby either the C content, the N content or the Nb/Ti ratio is varied. d-NaCl indicates a defective NaCl-type structure; enthalpies are in electron-volt per formula unit (f.u.). It is known that the transition monocarbides MC (M = Ti, Nb, V, etc) can exhibit carbon deficiency, and that their lattice parameters vary with the carbon concentration [19]. As summarized by Nagakura and S. Oketani [31], the lattice parameter of NbC_x is about 4.433 Å for $x = 0.82$, and 4.470 Å for $x \sim 1.0$. Our calculated lattice parameter for NbC is slightly larger (less than 1%) than the experimental value. This is not unusual for the DFT-GGA approximation which gives high-accuracy formation energies, but tends to overestimate the lattice parameters.

Considering the formation energies of the NbC_x phases (group A) as listed in Table 4, it is clear that carbon deficiency is energetically favourable for the composition range between $NbC_{0.50}$ and $NbC_{0.75}$. Here the formation enthalpy of $NbC_{0.50}$ is considerably lower ($\Delta H^2 = 0.46$ eV/f.u.) than that of $NbC_{0.75}$ ($\Delta H^2 = 0.02$ eV/f.u.), however the structure of $NbC_{0.50}$ is perfectly ordered (implying zero configurational entropy) while the structure of $NbC_{0.75}$ does bring about configurational entropy. Therefore, at elevated temperatures where entropy plays a role, both compositions are expected to be energetically favourable with respect to pure NbC (which also has zero configurational entropy) and C in solution. Considering the lattice parameters, it is difficult to directly compare experimental and calculated values (a small deviation in the Nb/Ti ratio can have a relatively large effect on the lattice parameter deviation). However, the DFT calculations show *qualitatively* that carbon deficiency leads to a

considerable decrease of the lattice parameter. The experimentally determined lattice parameter for NbC_x in this work (a=4.36 ± 0.05 Å, Table 3) is significantly smaller than the experimental lattice parameter of stoichiometric $NbC_{1.0}$ [31], and therefore the precipitates studied in the current work are most likely deficient in carbon content.

In group B in Table 4, the Nb/Ti ratio within the composition $Nb_XTi_{4-X}N_4$ is varied. When considering the formation enthalpy ΔH^2_{form} (defined with respect to pure NbN, TiN), all values are positive, thus NbN and TiN have a negative entropy of mixing and the partial sum of the two components is always energetically more favourable than the compound. On the other hand, when taking the solutes in bcc Fe as reference ΔH^1_{form}, it is clear that the formation of mixed Nb,Ti compositions is always associated with an energy gain. Therefore, the mixed compositions are favourable with respect to the solute elements in fcc Fe, but are metastable with respect to phase separation into NbN and TiN. The composition $(Nb_1Ti_3)N_4$ is closest to the experimentally observed Ti/Nb ratio of 2.83 ± 0.81. In group C of Table 4, the N content was varied for this composition $Nb_{0.25}Ti_{0.75}N_Z$ with 0<z<1. From the values of ΔH^2 in the Table, it is clear that N deficiency is never favourable. The calculations show qualitatively that the lattice parameter of the compound $Nb_{0.25}Ti_{0.75}N_{0.25}$ phase (8.35 Å) is smaller than twice the lattice parameter of NbN and TiN (4.26 Å and 4.45 Å, respectively, group B of Table 4), and that the lattice parameter decreases with decreasing N content. In combination with the literature values for the lattice parameters of NbN, TiN, this indicates that the experimentally observed precipitates are likely deficient in N content.

The question now arises why the calculations predict that Nb/Ti mixing is not favourable, while it is observed experimentally, and second why N deficiency is predicted to be not favourable while it is observed experimentally. Here the most important difference between experiment and the calculations is that the calculations are performed for a temperature of 0 K and zero pressure, while the precipitates are formed at high temperatures of 1500-1700 K in steel [9,34]. At these high temperatures, the entropy S contributes very significantly to the free energy as $F = H - TS$. Both Ti/Nb mixing, and N deficiency would contribute to configurational entropy at elevated temperatures. In addition, at these high temperatures the steel is no longer ferritic, but austenitic so that the reference point for the formation enthalpies (now calculated with respect to the solute elements of Nb, Ti, N, C in bcc Fe) is also not valid at those temperatures. Finally, the calculations are valid for bulk phases, while for precipitates interface energies and strain fields between the precipitate and the matrix are also of importance. The main conclusion that can be drawn from the calculations on the formation enthalpies, is that the carbon-deficient NbC_x precipitate phases (with $0.50<x<0.75$) are stable at low temperatures (0K to room temperature), while the $Nb_xTi_yN_z$ phases are metastable at low temperatures, both with respect to phase separation into TiN and NbN, and with respect to N deficiency.

4. Conclusions

In this work we have investigated microstructures and precipitates in a microalloyed multiphase steel containing ferrite, bainite, martensite and retained austenite. Precipitates were observed in the ferrite, martensite and bainite phases, but not in the austenite phase. Two kinds of precipitates were found in this steel: (Nb,Ti)N and NbC. (Nb,Ti)N precipitates were found in different sizes, ranging from 10-150 nm,

whereby the larger precipitates have a Ti/Nb ratio of approximately 2.83 ± 0.81 and were faceted in shape. Smaller NbC precipitates were found in a size range of 5-20 nm. The (Nb,Ti)N precipitates have a well-defined *Nishiyama Wasserman (N-W)* orientation relationship with the ferrite matrix, while the NbC precipitates are in random orientations. Both NbC and (Nb,Ti)N carbide precipitates are expected to take part in strengthening of these steels. The comparison of calculated lattice parameters and experimental lattice parameters indicates that both precipitates are deficient in carbon and nitrogen contents.

References

[1] Pereloma EV, Timokhina IB, Hodgson PD. Mater. Sci. Eng. A 1999; 273–275: 448–52.

[2] Pereloma EV, Timokhina IB, Russell KF, Miller M.K. Scripta Mater 2006; 54: 471–76.

[3] Sugimoto KI, Muramatsu T, Hashimoto SI, Mukai Y. J. Mater. Process. Technol 2006; 177: 390–95.

[4] Bleck W, Frehn A, Kechagias E, Ohlert J, Hulka K. Mater. Sci. Forum 2003; 426: 43–48.

[5] Pereloma EV, Russell KF, Miller MK, Timokhina IB. Scripta Mater 2008; 58: 1078–1081

[6] Hong SG, Kang KB, Park CG. Scripta Mater 2002; 46:163

[7] Wang HR, Wang W. J Mater Sci 2009; 44:591–600.

[8] Dutta B, Palmiere EJ, Sellars CM. Acta Mater 2001; 49: 785–94.

[9] Moon J, Lee C. Acta Mater 2009; 57: 2311–2320.

[10] Weiss I, Jonas JJ. Metallurgical Trans. A 1979; 10A: 831-840.

[11] De AK, Speer JG, Matlock DK. Adv. Mater Proc 2003; 161: 27–30.

[12] Sugimoto KI, Kobayashi M, Yasuki SI Metallurgical Trans A 1997; 28A: 2637-2644.

[13] He Y, Godet S, Jonas JJ. J. Appl. Cryst. 2006; 39: 72–81.

[14] Dieter G.E., Mechanical Metallurgy, third ed., New York: McGraw-Hill; 1988.

[15] Fujita N, Ohmura K, Yamamoto A. Mater Sci Eng A 2003; 351: 272–81.

[16] Sim GM, Ahn JC, Hong SC, Lee KJ, Lee KS. Mater Sci Eng A 2005; 396: 159–65.

[17] Silva CC, Farias JP, Miranda HC, Guimarães RF, Menezes JWA, Neto MAM. Mater Charact 2007; 59: 528-533.

[18] Smith WF. Structure and Properties of Engineering Alloys, second ed., New York: McGraw-Hill; 1993.

[19] Goldschmidt HJ. J. Iron steel inst. 1948; 160: 345.

[20] Kresse G, Hafner J. Phys. Rev. B 1993; 47: 558.

[21] Kresse G, Hafner J. Phys. Rev. B 1994; 49: 14251.

[22] Kresse G, Furthmüller J. Comput. Mat. Sci 1996; 6: 15.

[23] Blöchl PE. Phys. Rev. B 1994; 50: 17953.

[24] Kresse G, Furthmüller J, Phys. Rev. B 1999; 54: 1758.

[25] Perdew JP, Burke K, Ernzerhof M. Phys. Rev. Lett 1996; 77: 3865.

[26] Monkhorst HJ, Pack JD. Phys. Rev. B 1976; 13: 5188.

[27] SGTE Unary Database version v4.4, 20 July 2001. see. E.g. Elements and binary systems from Ag – Al to Au to Tl, in Thermodynamic Properties of Inorganic Materials, Eds. P. Franke and D. Neuschültz, Landolt-Börnstein: New Series Group 4: Phys. Chem. Vol 19 XXVI, Scientific Group Thermodata Europe (SGTE), (Springer, Berlin, 2002).

[28] Fang CM, van Huis MA, Sluiter MHF, Zandbergen HW. Acta Mater 2010; 58: 2968.

[29] Fang CM, van Huis MA, Sluiter MHF, Zandbergen HW. Phys. Rev. Lett 2010; 105: 055503.

[30] Fang CM, van Huis MA, Zanbergen HW. Scripta Materialia 2011, 64: 296.

[31] Nagakura S, Oketani S. Transactions ISIJ. 1968, 8: 265.

[32] Aigner K, Lengauer W, Rafaja D, Ettmayer P. Journal of Alloys Compd. 1994, 215: 121.

[33] Treece RE, Osofsky MS, Skelton EF, Qadri SB, Horwitz JS, Chrisey DB. Physical Review Serie 3. B - Condensed Matter. 1995, 51: 9356-9359.

[34] Buscaglia V, Martinelli A, Musenich R, Mayr W, Lengauer W. J. Alloys Comp. 1999, 283: 241.

Tables

Table 1: Overall chemical composition (wt.%) of the TRIP-assisted MP steel.

C	Mn	Si	Al	Cr	Nb	V	Ti	Ni	Cu	P	S	N
0.149	2.061	0.392	0.620	0.515	0.022	0.004	0.006	0.024	0.017	0.011	0.002	<0.0001

Table 2: Presence (+) and absence (−) of precipitates in the various steel phases.

Phases	**(Nb,Ti)N**	**NbC**
Ferrite	+	+
Martensite	+	−
Bainitic ferrite	+	−
Austenite (filmy)	−	−
Austenite (blocky)	−	−

Table 3: Experimentally obtained lattice parameters and calculated lattice mismatch in three directions between values for α-Fe, (Nb,Ti)N, and NbC.

Lattice parameter	(Nb,Ti)N	$a = 8.09 \pm 0.05$ Å
	NbC	$a = 4.36 \pm 0.05$ Å
	α-Fe	$a = 2.86$ Å
Lattice mismatch	[100] α-Fe // [110] (Nb,Ti)N	$\eta = 0.0$ %
	[011] α-Fe // [$\bar{1}$11] (Nb,Ti)N	$\eta = 15.5$ %
	[0$\bar{1}$1] α-Fe // [1$\bar{1}$2] (Nb,Ti)N	$\eta = 18.4$ %
	[100] α-Fe // [100] NbC	$\eta = 23.8$ %
	[100] α-Fe // [110] NbC	$\eta = 7.8$ %

Table 4. Calculated lattice parameters and formation enthalpies of NbC, NbN, TiN, and (Nb,Ti)N-type phases. The formation enthalpies ΔH_{form} are defined in Eqs. (5, 6) of the main text. Three groups of precipitate phases are considered, whereby either the C, N content or the Nb/Ti ratio is varied. d-NaCl indicates a defective NaCl-type structure; energies are in electron-volt per formula unit (f.u.). The phases with composition close to the experimentally found compositions are indicated with an asterisk (*).

Compound		Structure type	Latt. pars. ($\text{\AA}$)	$\Delta H^1_{\text{form.}}$ (eV/f.u.)	$\Delta H^2_{\text{form.}}$ (eV/f.u.)
A. NbC_x					
NbC_1		NaCl	$a = 4.506$	-1.489	0.000
$NbC_{0.75}$	(*)	d-NaCl	$a = 4.470$	-1.028	-0.021
$NbC_{0.50}$		d-NaCl	$a = 4.417^a$	-1.187	-0.456
$NbC_{0.25}$		d-NaCl	$a = 4.354$	-0.053	+0.247
$NbC_{0.00}$		Fcc-Nb	$a = 4.232$	+0.451	+0.451
B. $(Nb_xTi_{4-x})N_4$					
$(Nb_0Ti_4)N_4$		NaCl	$a = 4.256$	-10.248	0.0
$(Nb_1Ti_3)N_4$		d-NaCl	$a = 4.309$	-9.256	+0.041
$(Nb_2Ti_2)N_4$		d-NaCl	$a = 4.363$	-8.280	+0.066
$(Nb_3Ti_1)N_4$		d-NaCl	$a = 4.404$	-7.297	+0.099
$(Nb_4Ti_0)N_4$		NaCl	$a = 4.453$	-6.444	0.0
C. $(Nb_2Ti_6)N_n$					
$(Nb_2Ti_6)N_0$		d-NaCl	$a = 8.236$	+5.681	+5.681
$(Nb_2Ti_6)N_1$		d-NaCl	$a = 8.301$	+1.870	+4.432
$(Nb_2Ti_6)N_2$	(*)	d-NaCl	$a = 8.350$	-2.053	+3.071
$(Nb_2Ti_6)N_3$		d-NaCl	$a = 8.413$	-5.073	+2.613
$(Nb_2Ti_6)N_4$		d-NaCl	$a = 8.472$	-8.268	+1.944
$(Nb_2Ti_6)N_5$		d-NaCl	$a = 8.452$	-11.406	+1.404
$(Nb_2Ti_6)N_6$		d-NaCl	$a = 8.487$	-13.522	+1.850
$(Nb_2Ti_6)N_7$		d-NaCl	$a = 8.619$	-16.173	+0.810
$(Nb_2Ti_6)N_8$		d-NaCl	$a = 8.617$	-18.512	+0.082

[a]Half the value of a supercell with lattice parameter $2a$.

Figure 1
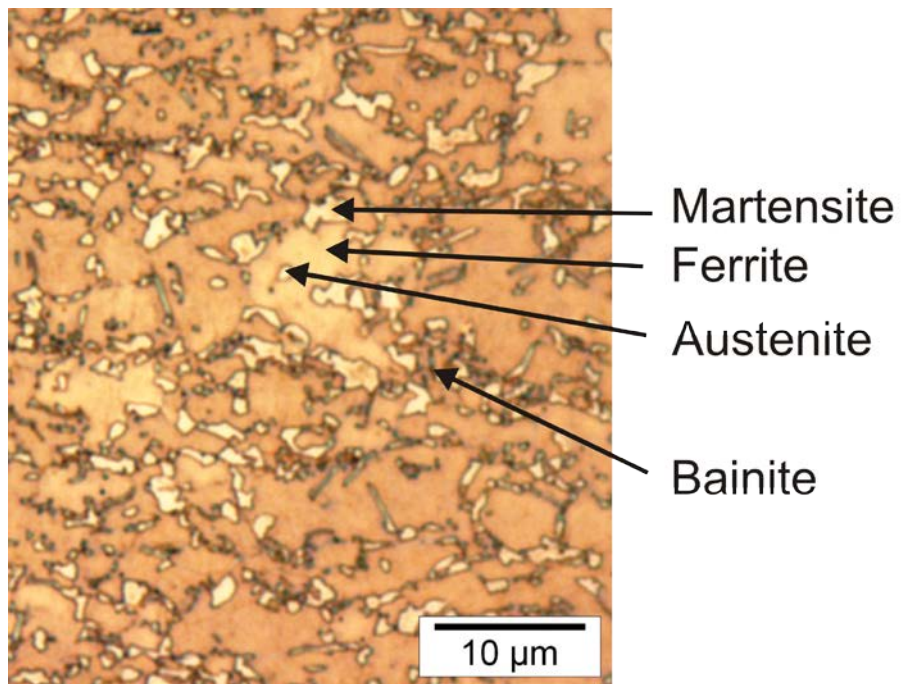
Figure 1. Optical microstructure of the TRIP-assisted MP steel.

Figure 2
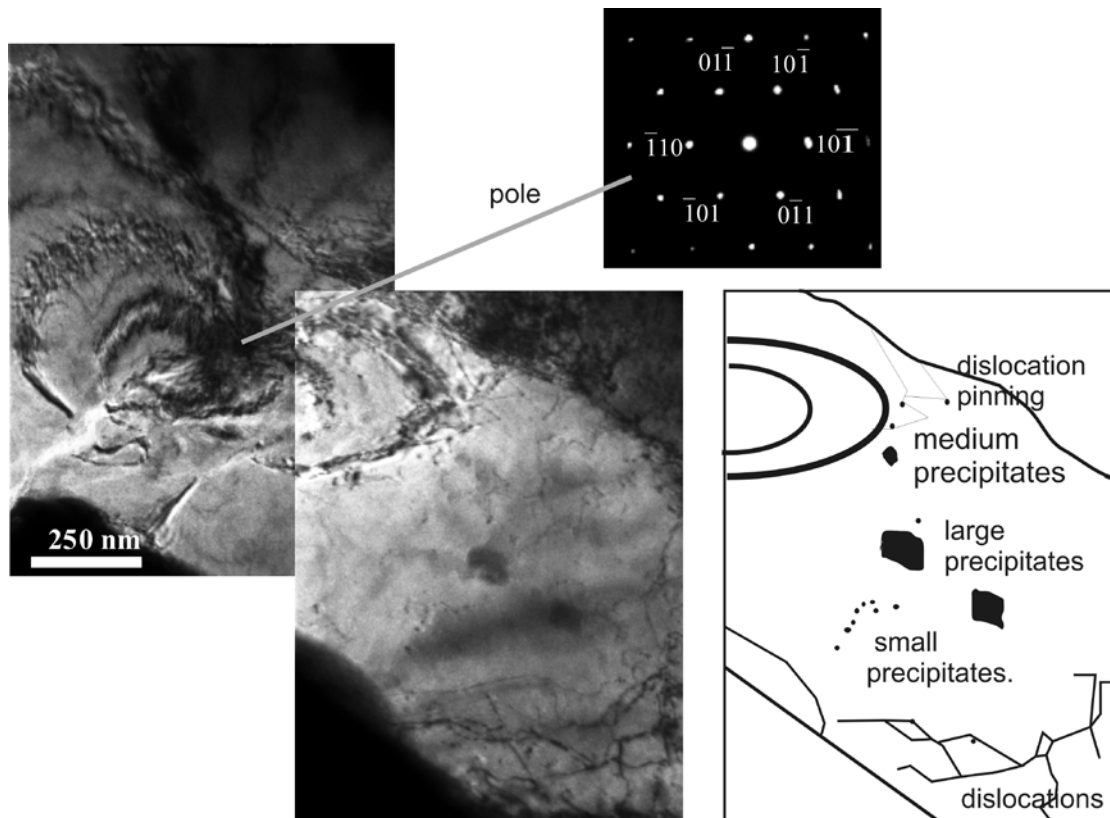
Figure 2. Ferrite in MP steel with precipitates and dislocations surrounding the precipitates. The features (indicated with arrows) are discussed in the text. The α-Fe $(1\bar{1}1)$ diffraction pattern is also shown.

Figure 3
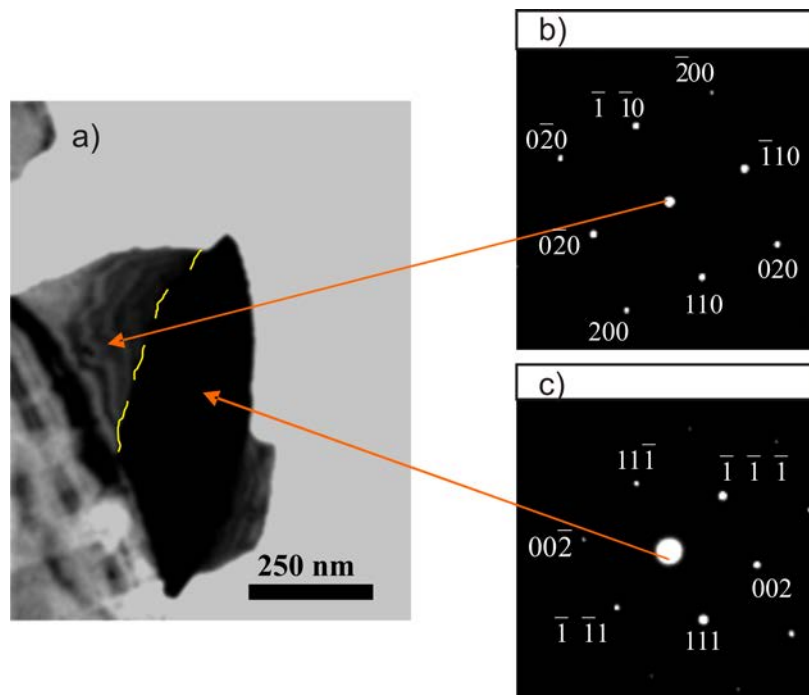
Figure 3. Blocky type austenite grain in MP steel which is close to the N-W relationship. a) bright-field TEM image. The boundary between the grains is indicated with yellow lines. b) diffraction pattern of ferrite in (001) projection. c) diffraction pattern of austenite in $(1\bar{1}0)$ projection

Figure 4
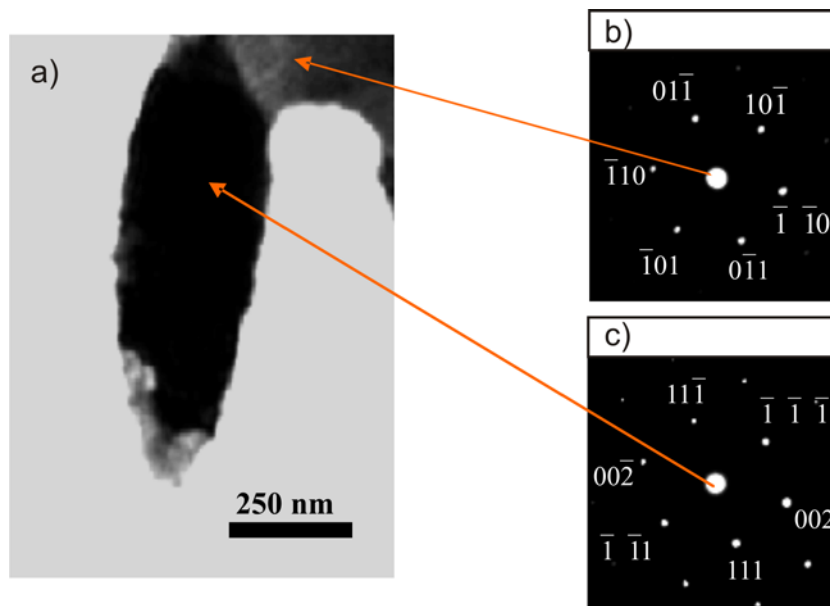
Figure 4. Filmy type austenite grain in MP steel with an orientation relation with the neighbouring ferrite grain that is close to the K-S relationship. a) bright-field TEM image. b) diffraction pattern of ferrite in (111) projection. c) diffraction pattern of austenite in $(1\bar{1}0)$ projection

Figure 5
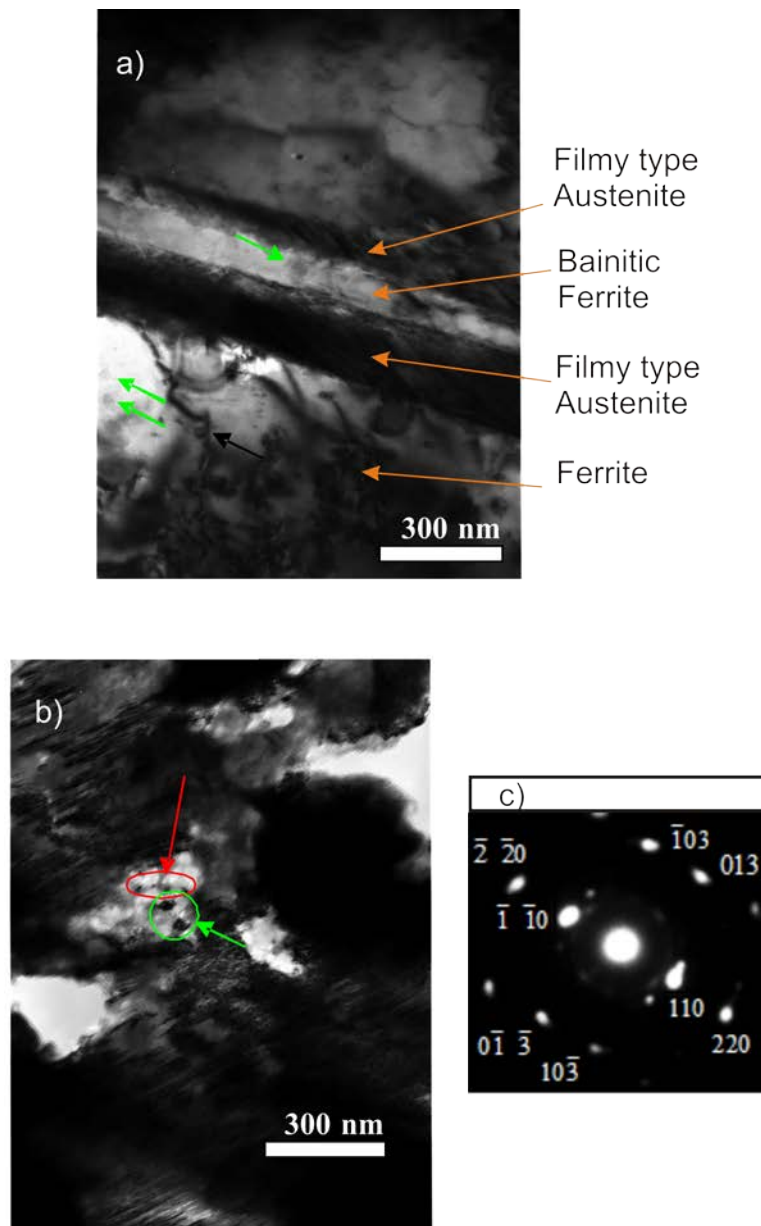
Figure 5. a) Bainite in MP steel with precipitates and dislocations in the surrounding ferrite grain. The phases within the bainite were identified by means of electron diffraction. b) Precipitates observed inside a grain of martensite. c) The inset shows diffraction pattern of martensite with the precipitates. Green arrows point to medium sized faceted precipitates and red arrow point to small sized precipitates.

Figure 6
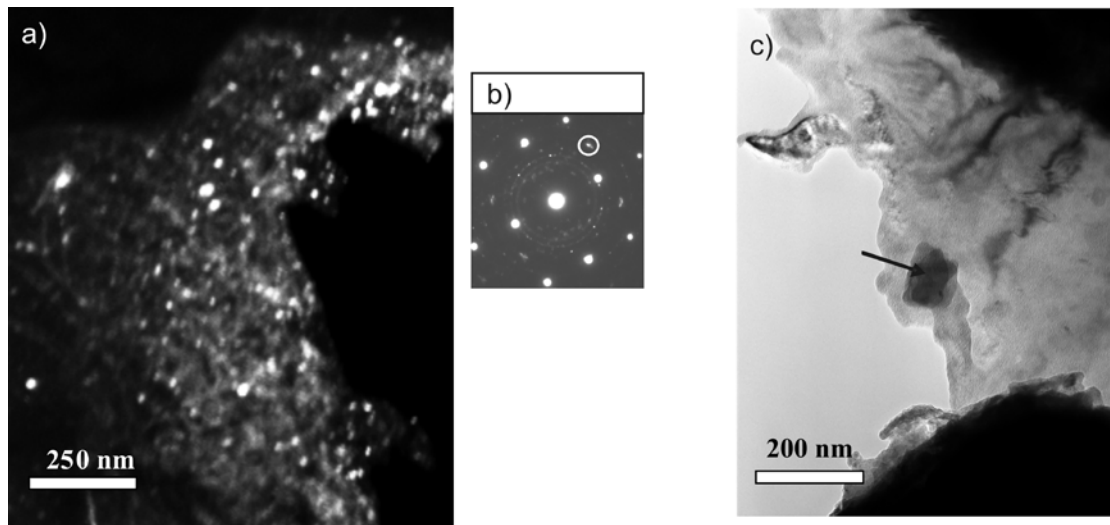
Figure 6. a) Dark field image showing (Nb,Ti)N precipitates in ferrite, using the g=404 reflection of (Nb,Ti)N. b) Corresponding diffraction pattern; the white circle indicates the g=404 reflection. c) A large (Nb,Ti)N precipitate inside a grain of ferrite.

Figure 7
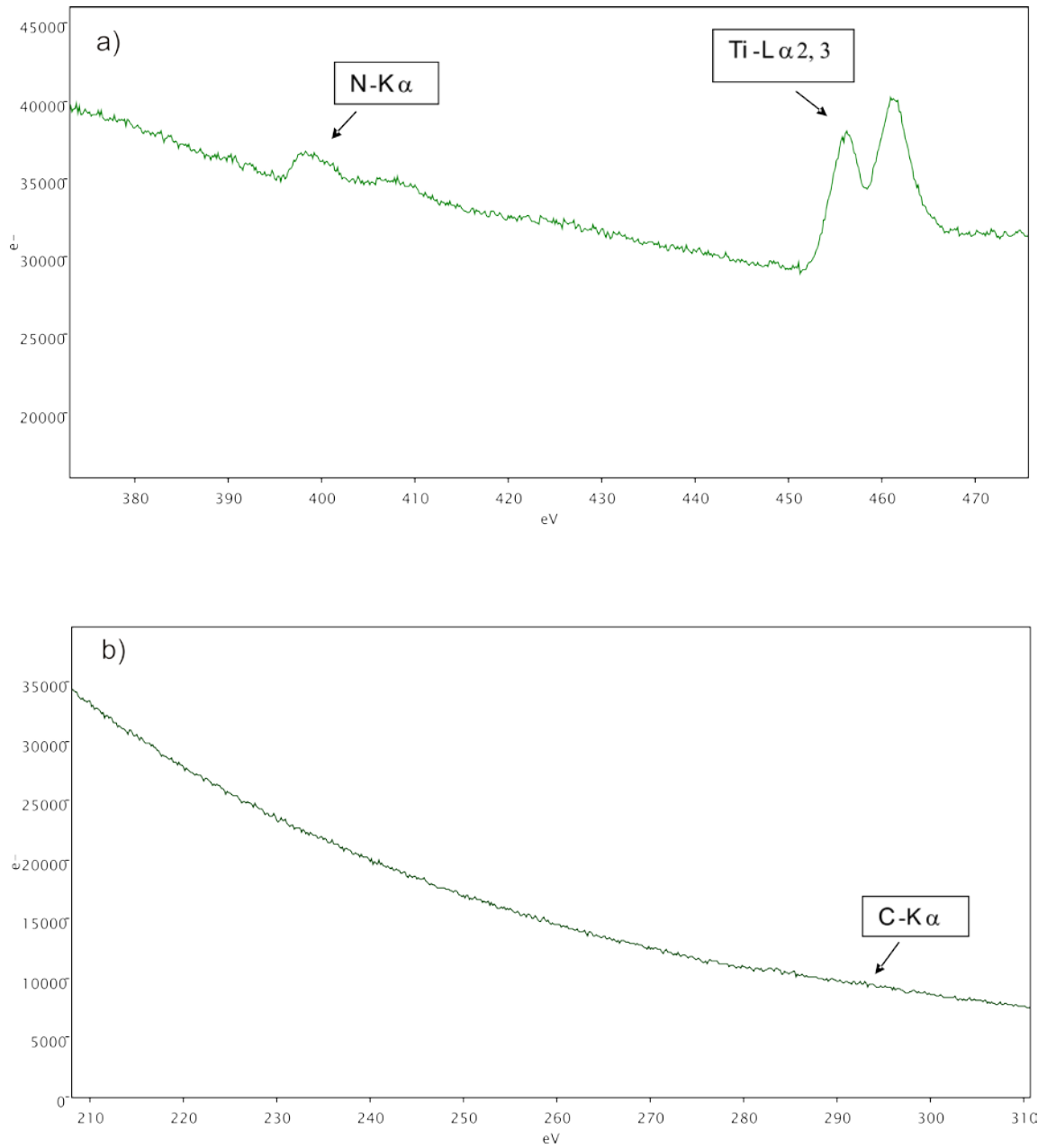
Figure 7. EELS analysis detecting (a) the presence of N in (Nb,Ti)N precipitates and (b) the absence of C in the (Nb,Ti)N precipitates.

Figure 8

Figure 8. Tilt series performed on a (Nb,Ti)N precipitate having an N-W relationship with the ferrite matrix. (a) The (Nb,Ti)N precipitate (magenata) is in a $(\bar{1}11)$ projection while α-Fe (orange) is in a (011) projection. b) The same (Nb,Ti)N precipitate (magenata) is in a $(\bar{1}1\bar{2})$ projection while α-Fe (orange) is in a (012) projection.
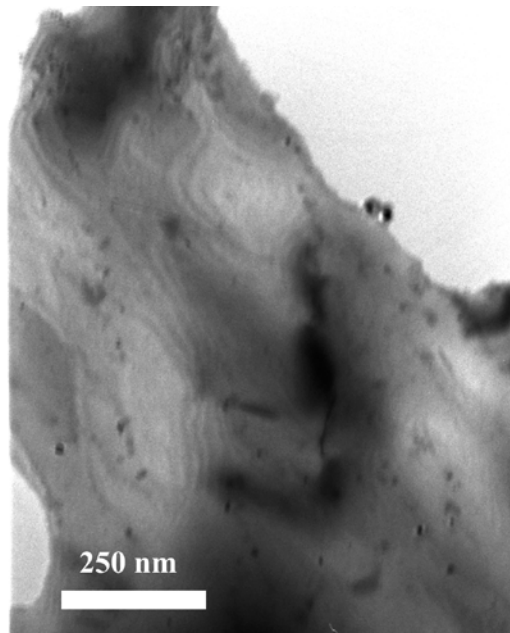
Figure 9

Figure 9: Several NbC precipitates inside a grain of ferrite.

Figure 10
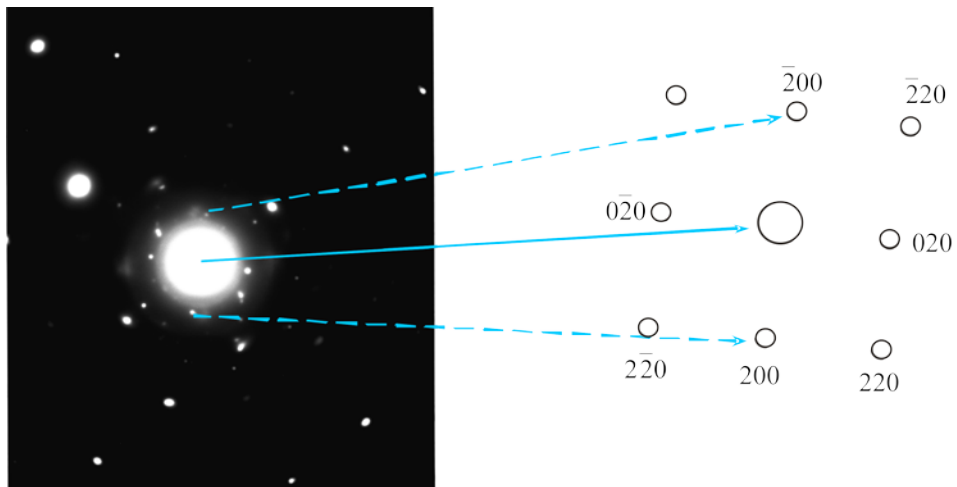
Figure 10: Electron diffraction pattern of NbC precipitates, some of which are in a near-(100) projection.